Investigating Natural Biofilms on Marine Microplastics and the Implications for Ocean Color Remote Sensing

Graham Richard Trolley

B.S., Cornell University, 2021

A Thesis

Submitted in Partial Fulfillment of the

Requirements for the Degree of

Master of Science

at the

University of Connecticut

2023

APPROVAL PAGE

Master of Science Thesis

Investigating Natural Biofilms on Marine Microplastics and the Implications for Ocean Color Remote Sensing

Presented by

Graham Richard Trolley, B.S.

Approved by
Major Advisor: Heidi Dierssen
Associate Advisor: Amir Ibrahim
Associate Advisor: Samantha Siedlecki

University of Connecticut

2023

Acknowledgements page

The completion and presentation of this master's thesis would not have been possible without the valuable input of many friends and colleagues. First and foremost, I'd like to thank my advisor, Dr. Heidi Dierssen, for her consistent enthusiasm towards my work and for the time and energy she devoted towards developing both my research project and my technical skills. I also deeply appreciate the numerous opportunities to travel, present, and collaborate with other researchers in the broader Ocean Color community that she's enabled. Additionally, I'd like to thank my committee members, Dr. Amir Ibrahim and Dr. Samantha Siedlecki for offering their time and insight.

Thank you to fellow graduate student Tyler Griffin for all his help with the sequencing analyses, which included sample preparation, bioinformatic analyses, and methods writeup contributions. These analyses represent an exciting facet of our dataset and would not have happened without his help and expertise.

Next, I'd like to thank all the members of the Spaceborne Quantification of Ocean MicrO-Plastics (SQOOP) project, including Dr. Amir Ibrahim, Dr. Heidi Dierssen, Dr. Kirk Knobelspiesse, Oskar Landi, Dr. Jacek Chowdhary, Dr. Matteo Ottaviani for listening to research updates and contributing feedback at our monthly meetings. Funding acknowledgement goes to the NASA Ocean Biology and Biogeochemistry Program.

Thank you to the Sea Education Association (SEA) for the opportunity to participate in their research cruise, and thank you to all my shipmates for sharing this memorable experience with me. Also, thank you to Jessie Turner, Deb Schuler, Elizabeth Rawlinson, Janet LaFlamme, and Claudia Koerting for always being willing to help and for always having an answer for any question I had.

Finally, I'd like to thank my friends and family who have encouraged and supported me over the years, I'm so grateful for everything.

Table of Contents

Figures:

Abstract

Plastic debris in the marine environment has become increasingly abundant in recent decades, with estimates suggesting that as many as 12 million metric tons of plastic enter the ocean each year. Monitoring tools are not yet well developed to assess global distributions of these particles, and analyses are underway to assess current and future remote sensing capabilities for plastic detection. One previously unexplored characteristic of marine microplastics is the modification of spectral reflectance by natural marine biofilms. Surface floating microplastic pieces with natural biofilm were collected across 4700 km of the convergence zone in the North Pacific gyre in summer of 2022. Spectral reflectance was measured on biofilmed microplastics shortly after collection and the biofilm was separated and stored for 16S and 18S DNA sequencing, which determined the biofilm microbiome makeup. Similar to past studies, the dominant taxa of the biofilm microbiome included prokaryotic Proteobacteria and Bacteroidia, and eukaryotic red algae and fungi. The red algal genus *Tsunamia* alone accounted for 52.9% of overall relative abundance within the eukaryotic microbiome. This microbiome modified the spectral shape of reflectance of the microplastics primarily in visible (VIS) wavelengths related to photosynthetic pigment absorption. Biofilm had minimal impact on spectral reflectance in near infrared (NIR) and short wave infrared (SWIR) wavelengths (700-2500 nm) with prominent absorption features specific to plastic hydrocarbons. For example, band depth measurements at absorption features centered at 1215 and 1732 showed no significant difference between biofilmed and cleaned samples. These results indicate that biofilm will have little impact on remote sensing methods in the NIR and SWIR related to plastic detection, but biofilm absorption in the visible may impact retrieval of photosynthetic pigments such as chlorophyll-a in the open ocean. A linear mixing simulation was conducted to determine

how different concentrations of surface-floating microplastics will influence the retrieval of chlorophyll-a from space. Presently, microplastic concentrations measured in the Great Pacific Garbage Patch (~10^6 pieces km^{-2}) are two orders of magnitude lower than concentrations that would have a detectable influence on ocean color chlorophyll-a retrievals (~10^8 pieces km^{-2}).

1. Introduction

The abundance of plastic debris in the marine environment has grown exponentially in recent decades, which poses a threat to ocean ecosystems and a variety of commercially relevant species (Colton et al., 1974; Law, 2017; Lebreton et al., 2018). Interest in protecting these marine systems has stimulated marine plastic research, with development targeting the eventual creation of an Integrated Marine Debris Observing System (IMDOS) that leverages in-situ and remote sensing sampling techniques to assess the global abundance of near surface plastics (Maximenko et al., 2019). One challenge associated with quantifying marine plastic abundance is the diverse range of plastic piece shapes and sizes. To account for this, plastics have been operationally separated into two size classes: macroplastics, which include all pieces greater than 5 mm in diameter, and microplastics which includes pieces between 0.33 and 5 mm in diameter (Thevenon et al., 2015). Feasibility studies have been conducted for the detection of floating macroplastics from airborne and satellite imagery, which show promising results for isolating macroplastic hydrocarbon signal in drone and aircraft remote sensing data (Castagna et al. 2023; Garaba et al., 2018; Garaba and Dierssen, 2018; Topouzelis et al., 2019). At present no protocol has been developed for detecting floating microplastics in remote sensing imagery, so current knowledge of the abundance of microplastics in the surface ocean relies on in-situ microplastic surveys and numerical models (Hu, 2021).

Ocean microplastic monitoring has occurred in situ using near-surface net tows since the early 1970's, though historic datasets of this nature are typically sparse (Carpenter and Smith Jr, 1972; Maximenko et al., 2019). For instance, for the 42 year period between 1971 and 2013, a total of 27 floating marine debris surveys consisting of 11,854 individual net tows have been compiled (Van Sebille et al., 2015). These tows observed accumulation of surface microplastics

in the five ocean subtropical gyres. Concentrations in the subtropical gyres were commonly observed between 10^5 and 10^7 pieces/km^2, while concentrations in regions outside the gyres (such as the equatorial Pacific) regularly ranged between 10^2 and 10^4 pieces/km^2. Among the subtropical gyres, the North Pacific Subtropical Gyre has been found to possess the highest surface microplastic concentrations and, overall, the largest mass reservoir (Jambeck et al., 2015). As a result, this region has been termed "the Great Pacific Garbage Patch".

Sensitivity analyses have been conducted to assess the viability of marine microplastic detection from current and future satellite platforms. For example, a study by Hu (2021) evaluated whether a reflectance anomaly due to uniformly distributed surface microplastics could be detected by a Sentinel-2 MSI-like optical sensor that balances revisit time (2-3 days), signal-to-noise ratio (SNR=200) and spatial resolution (10-20 m) favorably for microplastic studies. This analysis found that the enhanced reflectance signal due to surface microplastics at their maximum recorded density is 60 times lower than the signal and 20 times lower than sensor noise required for detectability (Hu, 2021). In scenarios where the assumptions of the sensitivity analyses are violated, however, microplastics may still be detectable. For instance, where plastics are heavily concentrated, rather than uniformly distributed (windrows, ocean fronts, or small-scale eddy convergence zones), particles may be sufficiently dense for detection (Cózar et al., 2021). Additionally, sensors with higher spatial resolution and higher SNR have been developed for airborne platforms (e.g AVIRIS-NG, spatial resolution 0.6m, SNR=1000) and may have potential for detecting floating microplastics (Scafutto et al., 2021).

For the purposes of remote sensing in these scenarios and for enhancing existing spectral libraries, quantification of microplastic reflectance properties is a prerequisite. Currently, spectral libraries are available to describe wet and dry marine harvested microplastics and

microplastic polymer type (Garaba and Dierssen, 2017, 2020). Marine harvested microplastics exhibit four diagnostic absorption features in the Near Infra-red (NIR) and the Shortwave Infra-red (SWIR) at 931, 1215, 1417, and 1732 nm. Wet marine harvested microplastics have similar absorption features but overall lower reflectance values than dry microplastics.

Commented [GT1]: At very end, change to (e.g. garaba…)

These studies document the reflectance of dry archived marine-harvested microplastics and commercially available virgin pellets. Such samples do not include any contribution from the wide variety of epiphyte algal and bacterial species that make up biofilms on marine microplastics in the natural environment (Pinto et al., 2019; West et al., 2016; Zettler et al., 2013). Since the first analyses of microbial communities on marine plastic debris were published in 2013, more than 70 studies have characterized the biofilm community on plastics using PCR-based methods (Debeljak et al., 2017; Latva et al., 2021; Zettler et al., 2013). Prokaryote community composition is well documented, with the community being typically dominated by Proteobacteria (~70% relative abundance), Bacteroidetes (~10%) and Cyanobacteria (~20%) (Latva et al., 2021). Prokaryote community succession has also been assessed with time series analyses, which identified an abundance of Alphaproteobacteria during the early stages of substrate colonization, and an abundance of Gammaproteobacteria, Bacteroides, and Actinobacteria later (Latva et al., 2021; Wright et al., 2021). Eukaryotic community composition has only been reported in a subset of studies and is less well understood. Dominant taxa in Eukaryotic studies of biofilm composition often include red, green, and brown algae, in addition to diatoms, dinoflagellates, ciliates, and fungi (Latva et al., 2021).

While the effect of natural biofilms on the optical properties of marine microplastics has not yet been explored, optical properties of marine biofilms have been studied in the laboratory on glass, mud, and polycarbonate filters (Kazemipour et al., 2011; Marrs et al., 1999). Biofilms

grown on all three substrates were found to attenuate reflectance from the ultraviolet (UV) to visible wavelengths with absorption peaks occurring between 673 and 675 nm corresponding to the in-vivo signature of chlorophyll-a.

In order to understand the optical properties of floating microplastics found in high concentrations across the convergence zones of the central gyres, we conducted hyperspectral reflectance measurements of freshly-harvested microplastics from the Great Pacific Garbage Patch (GPGP) in the North Pacific central gyre. These measurements show characteristic elements of plastic and biofilm spectral signatures, and provide a functional endmember for quantifying microplastics as they appear in the environment. The biofilms present on these microplastics were sequenced for both prokaryotic and eukaryotic community composition to understand the nature of the organisms and whether they are photosynthetic. With this new biofilmed microplastic endmember, we examined reflectance from marine microplastics as a contributor to current ocean color algorithms. The current Color Index chlorophyll-a algorithm is examined using a mixed-pixel simulation, in order to determine at what concentration biofilmed microplastics will impact chlorophyll-a retrievals and whether such concentrations currently exist in the environment (Hu et al., 2019).

2. Methods

2.1 Sample Collection

Fresh microplastic samples for this study were collected during the Sea Education Association Plastics Expedition through the GPGP in the North Pacific gyre during the summer of 2022 (Appendix 1). The Sea Education Association (SEA) regularly conducts research cruises for undergraduates and faculty scientists through their SEA Semester program. These cruises have employed regular and consistent neuston tow sampling techniques since 1986 to quantify in-situ floating microplastic concentrations (Law et al., 2014, 2010). Hence, this SEA cruise in 2022 contributed to one of the longest running datasets of marine microplastic concentrations available.

Samples were collected via neuston net tows at 21 stations in and around the GPGP. The cruise departed Honolulu, HI on 6/25/2022, sailed north to 35 N, turned eastward through the GPGP, and turned south at the California current before concluding in San Diego on 7/24/2022 (Fig. 1). One station occurred per day for sample collection prior to entering the California current, with subsequent stations occurring approximately 250km from each other. Per SEA protocols, neuston tows were conducted using a 335 µm mesh, 1 m x 0.5 m Sea Gear neuston net towed along the air-sea interface (Appendix 2) (Law et al., 2014). At each station, the tow line length was adjusted to position the net opening approximately half above and half below the surface, allowing material within the upper 25 cm of the water column to be collected. The net was towed off the port neuston boom for approximately 30 min at a speed of 2 knots, which translates to a tow distance of ~1.8 km. After each tow, the net was rinsed with seawater into a bucket, and plastics were manually removed from other neuston material. Plastics were stored in

seawater petri dishes indoors, away from direct sunlight until sampled for optical properties to minimize deterioration of biofilms.

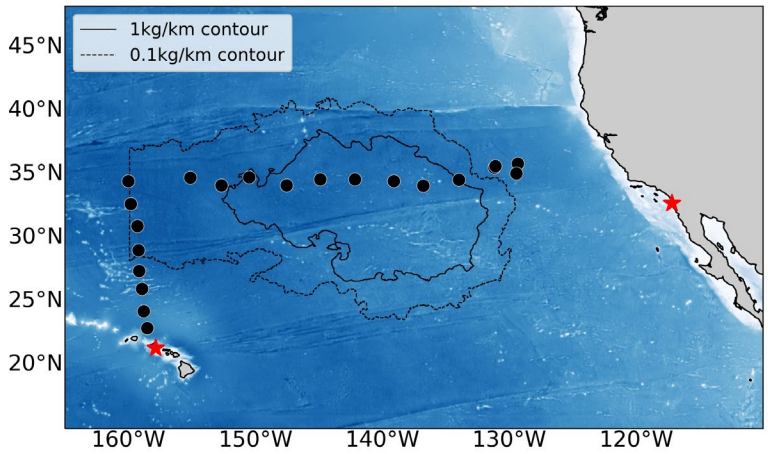

Figure 1: Map of plastic sampling locations visited for this study during the Sea Education Association (SEA) Summer 2022 cruise. Inner and outer GPGP contour definitions from Lebreton et al. 2017 are overlain for context.

2.2 Data Collection

Reflectance measurements of the damp, biofilmed microplastic samples were conducted at midday +/- 3 hrs, on deck using an Analytical Spectral Devices (ASD) Fieldspec-4 wide-res spectroradiometer equipped with an 8 degree FOV foreoptic. The use of natural skylight as the light source allowed for high signal-to-noise measurements in the UV-SWIR, with the exception of the 1350-1410 nm and 1800-1950 nm regions, in which the atmosphere is opaque.

Microplastic samples from a single net tow were aggregated into 5 cm diameter optically dense clusters on a dark (<2% reflectance in VIS-SWIR) felt background (Appendix 3). For optimizing the spectroradiometer's integration time, we utilized a 99% Spectralon® Lambertian

plaque (Labsphere, USA). Reflectance measurements were made by normalizing the upwelling irradiance to the downwelling irradiance. Downwelling irradiance was determined by measuring the Spectralon plaque (Castagna et al., 2019), normalized to the plaque's most recent spectral calibration (Dierssen, 2019). Upwelling irradiance was determined by measuring the aggregated plastics.

The measurement procedure involved three steps: A spectra was recorded over the plaque, followed by 10 measurements from different positions over the aggregated microplastic target, followed by another measurement over the plaque. For each microplastic aggregation, this measurement procedure was conducted three times with the microplastic pieces being gently stirred in between, to expose different surfaces of the pieces and obtain the most accurate bulk signal.

After initial optical processing, plastics were processed to remove and preserve non-encrusting biofilms. First, aggregated plastics were placed in 50mL conical centrifuge tubes with 35 mL of DI water. They were then shaken for 5 minutes, which dislodged biofilm constituents from the surface of the plastics. Then, the plastics were removed from the mixture via a coarse filter, leaving the biofilms suspended in DI water behind. This mixture was moved to a 60mL syringe with filter pad tip, loaded with a pre-weighed 25 mm, 0.7 μm mesh glass-fiber filter (GFF). The mixture was filtered, and the filter pads carrying biofilm material were immediately frozen.

The mass of biofilm on groups of aggregated plastics was determined for 17 samples. This was done by computing dry mass of biofilm per dry mass of microplastic (mg/g) for each aggregated microplastic sample. Biofilm dry mass for each sample was determined by taking the mass of the corresponding filter pad with biofilm after drying at 50°C for 24 hrs, then subtracting

the initial filter pad weight, and microplastic dry mass was determined by taking the mass of the aggregated pieces after drying.

After biofilm removal, the cleaned, damp plastics were reprocessed for reflectance measurements on the ship, using the same sampling procedure described for the biofilmed microplastics. They were then dried and stored. Once on shore, they were processed again for dry reflectance at the UConn Avery Point campus.

2.3 Spectral Data Processing

Reflectance spectra provide information about what fraction of light is reflected by a target at a given wavelength. Individual spectra may contain spectral features such as absorption bands and reflectance peaks, which govern spectral shape and inform on target identity. Differences between characteristic target spectra (known as spectral endmembers) can be used to distinguish different targets, which forms the basis for spectral mixture analysis (Somers et al., 2011).

For the microplastic samples, reflectance spectra were calculated by normalizing individual measurements over the aggregated pieces to the average downwelling irradiance determined from the plaque measurements taken before and after. In some cases, microplastic reflectance spectra exhibited a discontinuity at 1000 nm, which corresponds to the transition between the ASD fieldspec 4 VNIR and SWIR1 detectors. This type of discontinuity has been linked to spectral sensitivity drift arising from temperature effects and inhomogeneities within the sensor field of view. Discontinuities were corrected for using a step correction approach (Hueni, A. and Bialek, A., 2017; Khan et al., 2021). Spectral reflectance endmembers for biofilmed, cleaned, and dry microplastic were then determined by averaging the corresponding discontinuity-corrected spectral reflectance measurements.

To understand biofilm optical properties, biofilm absorptance spectra were estimated from the reflectance data. Generally, absorptance characterizes how light is absorbed by a system, and is calculated as the ratio of the radiant flux absorbed by a sample to the incident radiant flux (Kirk, 1994). Here, an average biofilm absorptance spectra was determined as the difference between the cleaned and biofilmed reflectance endmember spectra, as described in (Khan et al., 2021).

Band depth is a widely-used metric for studying the relative strength of spectral absorption features, and is calculated by taking the difference between the continuum reflectance and the reflectance at the absorption band center, normalized to the continuum reflectance (Clark and Roush, 1984). Band depth was calculated for each microplastic reflectance spectra at 673 nm which corresponds to the in-vivo, red absorption peak of chlorophyll-a, and at 931, 1215, and 1732 nm, which correspond to characteristic absorption features of floating marine microplastics (Garaba et al., 2018; Kazemipour et al., 2011). Band depth is not reported for the 1417 nm microplastic absorption feature because of the poor SNR at these wavelengths due to atmospheric absorption. Differences between sets of band-depth values at each wavelength between the biofilmed and cleaned spectra were determined using the Kolmogorov-Smirnov statistical test, which reports how likely it is to obtain two different sets of measurements if they were drawn from the same but unknown probability distribution.

Spectral angle is common metric for assessing the similarity in spectral shape between two spectra, which treats two input spectra (x, y) as vectors and calculates the angle between them, reported as an angle between 0 and 90°, according to (Kruse et al., 1993):

$$\boldsymbol{\theta = cos^{-1}\frac{\Sigma xy}{\sqrt{\Sigma x^2 \Sigma y^2}}}$$

This metric has been used in the past to assess the similarity of spectra within groups by reporting the mean and standard deviation of spectral angle for each pair of spectra within a category. The resulting spectral angle similarity was interpreted with a scale as very strong ($0° \leq \theta \leq 5°$), strong ($5° < \theta \leq 10°$), moderate ($10° < \theta \leq 15°$), weak ($15° < \theta \leq 20°$) and very weak ($20° < \theta$) (Garaba and Dierssen, 2018). Recently, spectral angle variability has been implemented to assess variability both within a group of endmembers, and between two different groups of endmembers (Frye, 2023). This approach was implemented here by calculating the mean spectral angle for each unique pairwise combination of spectra within (intra) and between (inter) the biofilmed and cleaned groups of spectra. These were calculated for the full spectrum, and separately for the VIS (400-700 nm), NIR (700-1350 nm), and SWIR (1410-2350 nm) regions of the spectrum.

2.4 Microbiome Analyses

Ten filter pads across GPGP were processed to prokaryotic and eukaryotic community composition based on ASV relative abundance. In the context of standard microbial analyses, this is considered a small sample size with limited replicates. However, the goal of this study is to provide an overview of dominant taxa as context, and not to rigorously define the biofilm community at ocean basin scales.Filter pads were chosen to encompass the full longitudinal range of this study and were processed with prokaryotic (16S) and eukaryotic (18S) microbiome analyses (Fig. 2). The ZymoBiomics DNA Miniprep Kit (Zymo Research Corp., Orange County, CA) was employed to extract total genomic DNA from the ten filters, following the manufacturer's instructions, with the inclusion of a proteinase K (20 mg/ml) digestion at 55°C for 15 min. DNA samples were submitted to LC Sciences, LLC (Houston, TX) for amplification

and sequencing services. For prokaryotic analysis, 16S rRNA gene fragments (V3-V4 hypervariable region) of the extracted DNA were amplified with PCR using 341F (5'-CCTACGGGNGGCWGCAG-3') and 805R (5'-GACTACHVGGGTATCTAATCC-3') primers. Fragments were amplified using a Phusion Hot Start II Polymerase kit (Thermo Fisher Scientific, Waltham, MA). Reactions were incubated at 98°C for 30 s for initial denaturation. Reactions were then subjected to 35 cycles of 98°C for 10 s, 54°C for 30 s, and 72°C for 45 s, followed by a final elongation step of 72°C for 10 min. For each sample, amplification was confirmed visually by gel electrophoresis and imaged under UV. Amplification procedures were identical for the eukaryotic analysis, except for the use of 18S rRNA primers: 817F (5'-TTAGCATGGAATAATRRAATAGGA-3') and 1,196R (5'-TCTGGACCTGGTGAGTTTCC-3'). PCR products were isolated with 2% agarose gels, and purified with AMPure XT beads (Beckman Coulter Genomics, Danvers, MA). Following PCR, the amplicons were analyzed with an Agilent 2100 Bioanalyzer (Agilent Technologies, Inc., Santa Clara, CA) and KAPA Library Quantification Kits (Kapa Biosciences, Woburn, MA). Sequencing was performed on a NovaSeq 6000 platform, generating 2 x 250 bp paired-end reads.

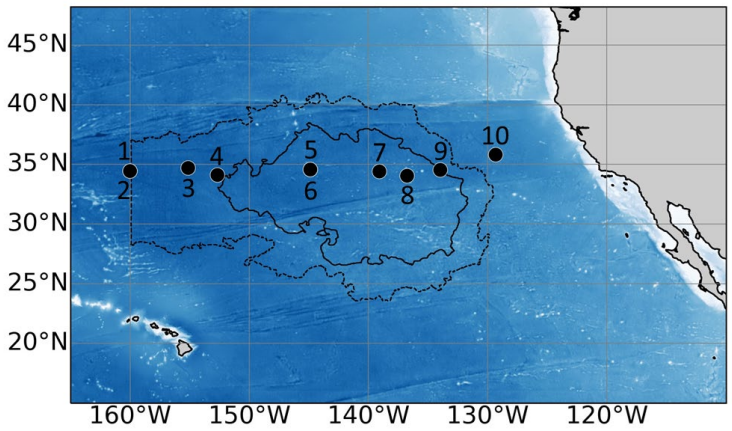

Figure 2: Map showing the sample locations for filter pads used in sequencing analyses. Inner and outer GPGP contour definitions from Lebreton et al. 2017 are overlain for context.

Bioinformatic amplicon sequence analyses for prokaryotic and eukaryotic data were conducted separately. A total of 829,698 raw reads (median 82,372.5 reads) and 842,692 reads (median 84,392 reads) from the 10 samples were loaded into the analysis pipeline for the prokaryotic and eukaryotic analyses, respectively. Paired-end reads were merged using FLASH (version 1.2.8; Magoč and Salzberg, 2011). Quality filtering on the raw reads was performed using specific filtering conditions via fqtrim (version 0.94; Pertea, 2018). Chimeric sequences were filtered using VSEARCH software (version 2.3.4; Rognes et al., 2016). Dereplication was accomplished with DADA2 (version 2019.7; Callahan et al., 2016). Taxonomic assignments to the species level, when possible, were conducted via alignment to the SILVA rRNA gene database (version 132; Quast et al., 2013). Further data analyses, manipulation, and figure generation were conducted with the phyloseq package (version 1.38.0; McMurdie and Holmes, 2013) and ggplot2 package (version 3.3.6; Wickham, 2016) in R (version 4.3.0). For the prokaryotic dataset, amplicon sequence variants (ASVs) with taxonomic assignments associated

with eukaryotes, chloroplasts, and mitochondria were considered erroneous and removed from the analysis. Data used downstream were not rarefied, and rarefaction was used only for evaluating sequence coverage. Prior to analyses of beta-diversity, variance stabilizing transformations were conducted with DESeq2 (version 1.34.0; Love et al., 2014) to correct for differences in library sizes (McMurdie and Holmes, 2014), and then Bray-Curtis dissimilarities were computed. Alpha-diversity was calculated using the Shannon index metric.

2.5 Remote Sensing Algorithms

In the open ocean environment, surface microplastics are currently an unparameterized optically active constituent with enhanced reflectance relative to the background water. As a result, their presence within a given pixel of ocean color data will change its measured color, and thus influence algorithms that use ocean color measurements. A linear mixing simulation was conducted to determine how much plastic subpixel fractional coverage, and subsequently plastic concentration, is required to observe a significant deviation in a widely used ocean color product: chlorophyll-a.

Remote sensing reflectance (Rrs) spectra were simulated for plastic subpixel fractional coverage (f_p) values between 10^{-5} and 10^{-1} (0.001% and 10%). It was assumed that all of the optically active plastic pieces in this simulated pixel were buoyant, so the simulated Rrs spectra was calculated via linear mixing of a plastic and water Rrs endmember, weighted by their subpixel fractional coverages. Simulations were conducted for both damp, biofilmed, and damp, cleaned microplastic pieces. The plastic Rrs endmembers were calculated as the average of the corresponding plastic reflectance measurements taken in this study, scaled by π. The water Rrs endmember used was determined as the average of 7 replicate water Rrs measurements taken on

the same cruise at 34°19.462’ N, 157°01.643’W in the north Pacific gyre. These measurements were made using the ASD fieldspec 4, according to the method outlined in (Mobley, 1999).

Chlorophyll-a was retrieved using the standard ocean color algorithm: Ocean Color Index (OCI). The OCI algorithm itself is a hybrid of 2 separate algorithms. The 3-band difference Color Index is used for low chlorophyll waters (Chl ≤ 0.25 mg m−3), the traditional band ratio algorithm OCx is used for high chlorophyll waters (Chl > 0.3 mg m−3), and a weighted mixture of the two algorithms is used for intermediate chlorophyll waters (Hu et al., 2019; O’Reilly and Werdell, 2019). The Color Index approach was used to simulate spectra in the oligotrophic GPGP. The Color Index algorithm requires blue, green, and red bands, which are selected as the nearest bands to 443, 555, and 670 nm, respectively. Band values were retrieved by convolving the simulated spectra to the nearest MODIS-Aqua bands based on their relative spectral response (NASA Ocean Biology Processing Group, 2023). From there, Chlorophyll-a was retrieved using the Color Index algorithm (Hu et al., 2019).

Models and in-situ measurements of marine plastics use plastic concentration (pieces km^{-2}) to describe plastic abundance, rather than fractional coverage at the surface. To convert between f_p and plastic concentration, measurements of individual microplastic piece length, width, and height were used (Garaba and Dierssen, 2018). It was assumed that the largest face of these pieces would be oriented upwards (thus contributing to the fractional coverage within a pixel), and that this face is approximately oval-shaped. From these data, the average upward-oriented area of a piece of sampled plastic was estimated to be 23.4 mm^2.

3. Results

Here, we describe the natural biofilm on marine microplastics, how the biofilm influences that spectral reflectance and absorptance of marine microplastics, and the impact of biofilm on ocean color remote sensing algorithms for monitoring microplastics and chlorophyll-a.

3.1 Biodiversity of Microplastic Biofilm

A total of 685,241 (82.6 %) and 811,833 (96.3 %) merged read-pairs passed the quality filtering and chimera detection and were passed to phyloseq for the prokaryotic and eukaryotic analyses, respectively. After filtering out ASVs with taxonomic assignments associated with eukaryotes, chloroplasts, and mitochondria, 2,681 ASVs were recovered in the prokaryotic dataset. There were 1,656 ASVs recovered in the eukaryotic dataset. Rarefaction analysis indicated that the sampling effort was satisfactory in capturing the true prokaryotic and eukaryotic ASV diversity in all ten samples (Appendix 4).

3.1.1 Beta Diversity

There were no strong geographic patterns of clustering for the ten prokaryotic and eukaryotic communities apparent from ordination of Bray-Curtis dissimilarities (Appendix 5). In general, however, communities sampled on the same day and at the same geographic location tended to cluster in tight proximity.

3.1.2 Alpha Diversity

There were no obvious trends in the Shannon diversity index, which considers both richness and evenness, for the prokaryotic or eukaryotic datasets across longitudes or position in the garbage patch (Appendix 6). The mean Shannon index value for prokaryotic communities

was 4.19 (SD = 0.591) with a low of 2.86 recovered in sample 4 and a high of 4.70 recovered in sample 6. The mean Shannon index value for eukaryotic communities was 2.38 (SD = 0.570) with a low of 1.56 recovered in sample 5 and a high of 3.41 recovered in sample 8. It is notable that for both alpha diversity metrics, mean diversity was higher in the prokaryotic communities than eukaryotic communities; prokaryotic communities had 130.4% higher mean ASV richness and 76.1% higher mean Shannon index values.

3.1.3 Taxonomic Composition

At the class-level, the prokaryotic communities tended to be dominated by ASVs assigned to the Gammaproteobacteria with 63.9 % mean relative abundance (SD = 20.83 %), with other notable contributions from ASVs assigned to the Alphaproteobacteria with 16.3 % mean relative abundance (SD = 7.49 %) and Bacteroidia with 14.7 % mean relative abundance (SD = 14.25 %; Fig. 3A). The prokaryotic communities of samples 5 and 6 were noteworthy for their marked evenness at the class-level. The eukaryotic communities tended to be dominated by ASVs assigned to class Stylonematophyceae with 53.0 % mean relative abundance (SD = 16.58 %; Fig. 3B). Mean relative abundance of ASVs assigned to class Hydrozoa was 7.4 % (SD = 10.06 %) with highest representation in samples 1 and 2 (21.9 % – 28.7 % relative abundance). Samples 1 and 2 were also notable for their near negligible relative abundance of ASVs assigned to class Microbotryomycetes, which had a mean relative abundance of 18.6 % (SD = 13.11 %) in the other eight samples.

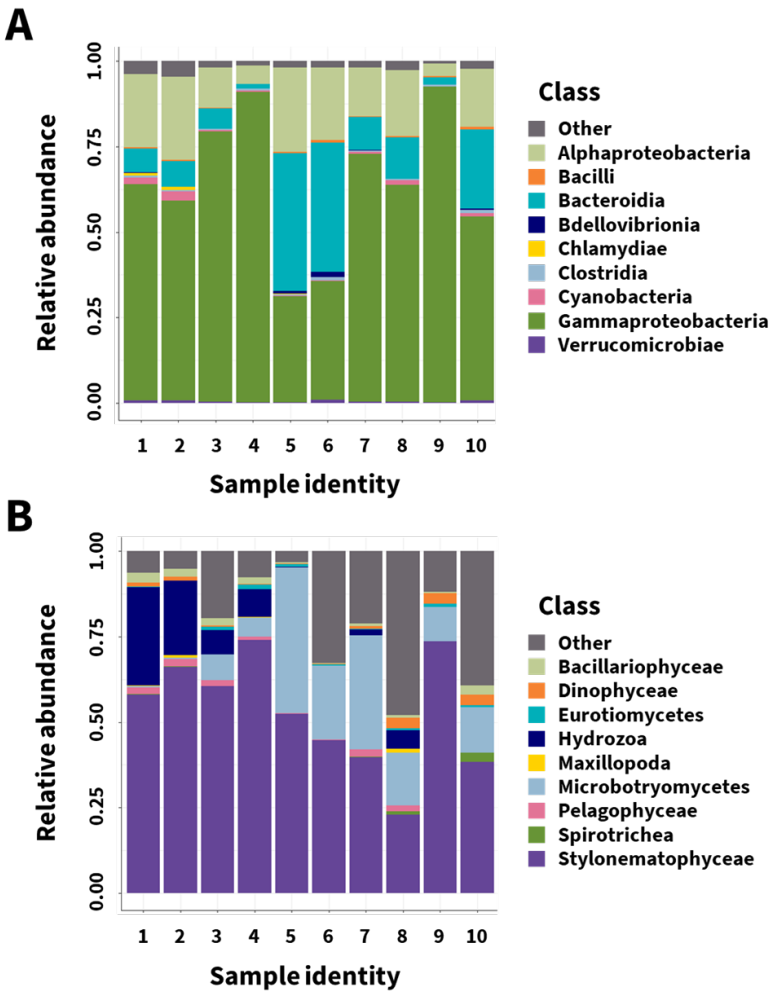

Figure 3: Relative abundance of amplicon sequence variants (ASVs) grouped at the class level for each sample in the prokaryotic analysis (A) and eukaryotic analysis (B). Several less abundant classes are grouped together as "other" in each panel for simplicity of viewing.

The most prominent prokaryotic genus to which ASVs were assigned was *Pseudoaltermonas* with 37.4 % mean relative abundance (SD = 19.31 %; Fig. 4A). Samples 5 and 6 had, again, notably high evenness at the genus-level. ASVs assigned to genus *Vibrio* made up 55.0 % of the prokaryotic community of sample 9, but otherwise had generally low mean relative abundance at 3.9 % (SD = 4.86 %) in the other nine samples. For the eukaryotic communities, the most dominant genus to which ASVs were assigned was *Tsunamia* with 52.9 % relative abundance (SD = 16.55 %; Fig. 4B). Samples 1 and 2 had the highest relative abundances of ASVs assigned to genus *Velella* while also having near negligible relative abundance of ASVs assigned to genus *Rhodotorula*, which had notable mean relative abundance in the other eight samples at 18.6 % (SD = 13.10 %).

ASV's were assigned to photosynthetic taxa other than *Tsunamia* with much lower mean relative abundances. These included prokaryotic taxa such as the phylum cyanobacteria at 1.0 % (SD = 0.5 %) and phylum Chloroplexi at 0.01 % (SD = 0.01 %), and eukaryotic taxa such as the class Bacillariophyceae at 1.5 % (SD = 1.03 %) class Dinophyceae at 1.3 % (SD = 1.28%), phylum Phaeophyceae at 0.03 % (SD = 0.04 %), and phylum Chlorophyta at 0.01 % (SD = 0.02 %).

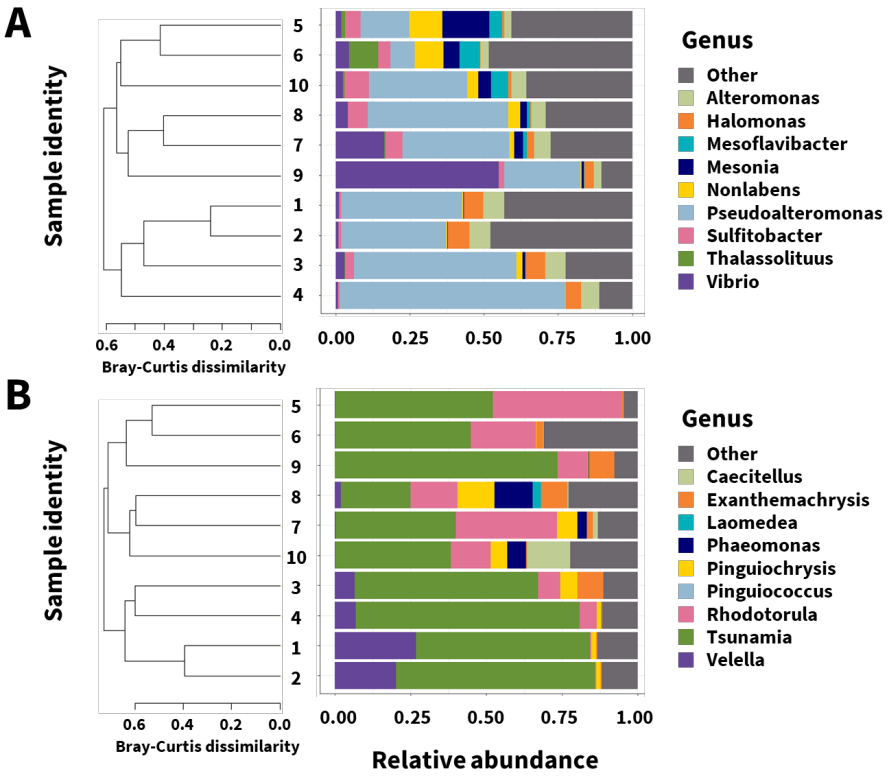

Figure 4: Relative abundance of amplicon sequence variants (ASVs) grouped at the genus level for each sample in the prokaryotic analysis (A) and eukaryotic analysis (B). Several less abundant classes are grouped together as "other" in each panel for simplicity of viewing. Dendrograms drawn using the unweighted pair group method with arithmetic mean (UPGMA) from Bray-Curtis dissimilarity matrices are shown to the left and provide the basis for sample ordering.

It should be noted that the method of collecting microplastics via neuston net tows used in this study invariably exposes the plastics to eDNA of other epipelagic organisms. For instance, samples from the western gyre (sample ID#1-4) showed significant relative abundances of Hydrozoans. At these same sites, neuston net tows captured by-the-wind sailors (*Vellela vellela*) alongside microplastics. Previous work has determined *Vellela vellela* do not have any substrate-

bound life cycle stages, so it is likely that this high relative abundance is due to the physical exposure of these plastics to these species during the collection process, rather than these hydrozoans being a major constituent within the plastic biofilm microbiome (Langstroth and Langstroth, 2000). The identification of every eDNA source is beyond the scope of this study, so future analyses will need to distinguish microbiome constituents from eDNA sources as needed.

3.1.4 Biofilm Mass

The dry mass of biofilm per dry mass of microplastic (mg/g) was determined for the aggregated microplastic samples not used for 16S and 18S sequencing (Appendix 7). The average biofilm mass for samples was 9.04 mg biofilm/g microplastic, with a standard deviation of 6.39 mg biofilm/g microplastic. The maximum observed value was 22.07 mg biofilm/g microplastic and the minimum was 0.2 mg biofilm/g microplastic.

3.2 Optical Properties

A total of 532, 468, and 63 reflectance measurements were made of aggregated damp biofilmed, damp cleaned, and dry microplastics respectively (Fig. 5). In general, the spectra showing monotonically increasing reflectance in visible wavelengths and peaking in the NIR. The spectra for all three groups also show distinct absorption features at the 931, 1215, 1417, and 1732 nm characteristic wavelengths for microplastics, and the cleaned and dry microplastic spectra have higher reflectance across the entire spectrum (Garaba et al., 2018).

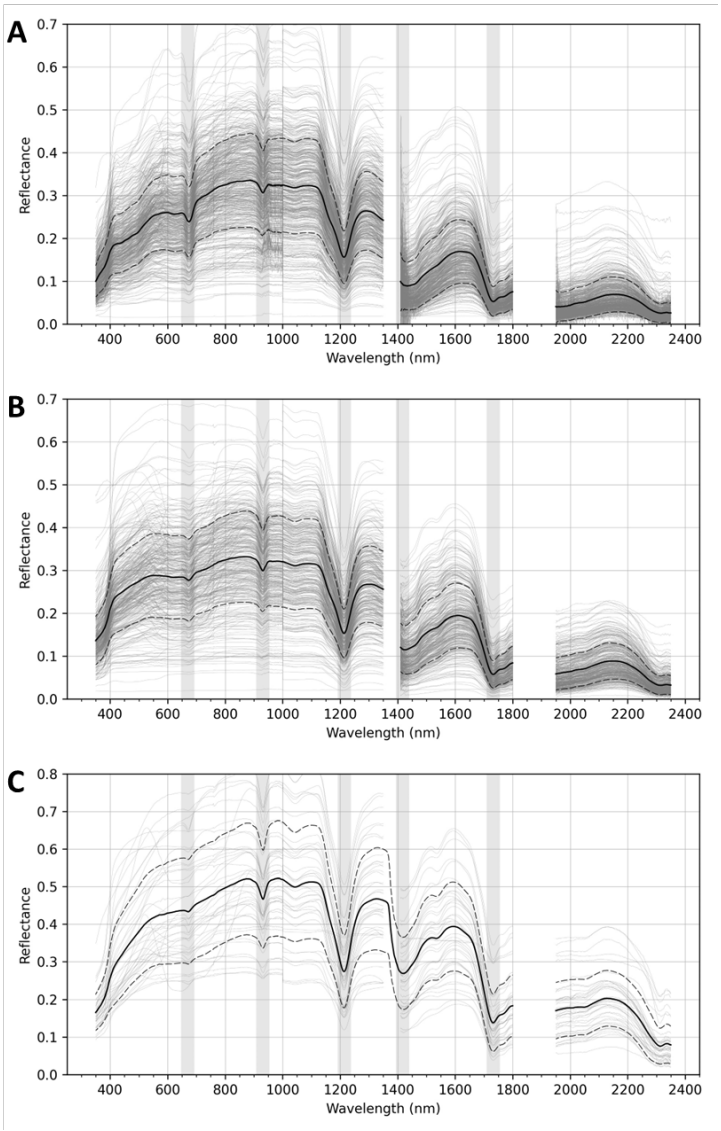

Figure 5: All aggregated microplastic reflectance measurements from damp, biofilmed (A), damp, cleaned (B), and dry (C) microplastic pieces. Grey bands indicate 673 nm chlorophyll-a absorption and the four characteristic plastic absorption features in the NIR/SWIR. Light grey spectra are the raw individual measurements, the black line is the average of all the individual measurements, and the dashed lines are +/- 1 Standard deviation.

Biofilmed and cleaned, damp microplastic reflectance endmembers generally increased through the VIS and NIR to a maximum at 890 nm and decreased into the SWIR (Fig. 6A). These endmembers deviate significantly at visible wavelengths, with the biofilmed endmember exhibiting lower reflectance magnitude and a significant absorption feature at 673 nm. The endmembers show similar magnitude moving into the NIR, and the biofilmed endmember shows lower magnitude in the SWIR.

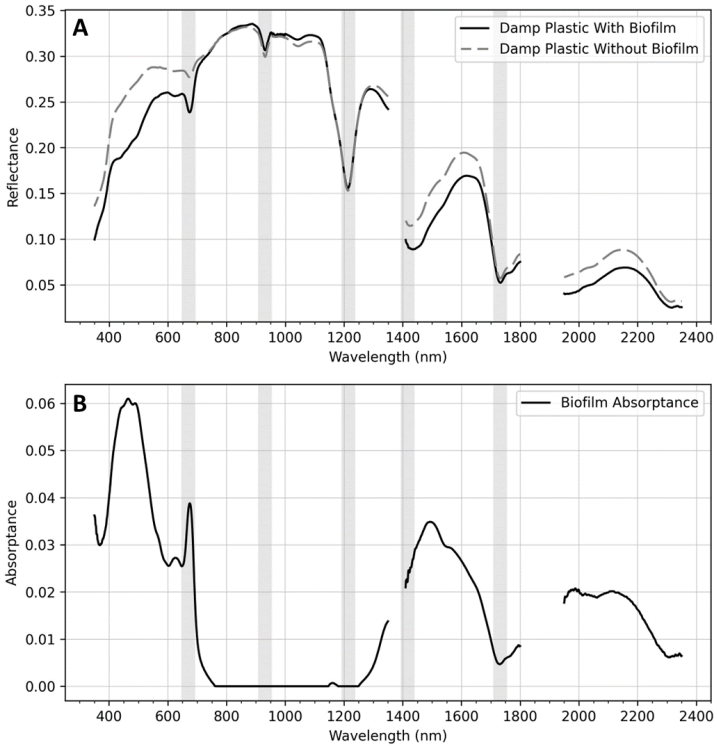

Figure 6: Average reflectance endmember spectra for damp biofilmed and cleaned plastic samples (A) and the average absorptance for the microplastic biofilm (B). Grey bands indicate 673nm chlorophyll-a absorption and the four characteristic plastic absorption features in the NIR/SWIR.

For all microplastic spectra, prominent absorption features are observed at the four wavelengths previously identified as characteristic plastic absorption bands (Fig. 5) (Garaba and Dierssen, 2018). In addition, biofilmed microplastics have a fifth band centered at 673 nm related to absorption by the pigment chlorophyll-a. When comparing the reflectance spectra from damp biofilmed and cleaned samples (e.g., Fig. 6A), the band depths at 1215 and 1732 nm were not found to be significantly different ($p>0.05$). However, band depths at 673 and 931 nm were found to be significantly different ($p<0.05$) between the biofilmed and cleaned groups of reflectance spectra based on the Kolmogorov-Smirnov statistical test.

Spectral angles were computed for spectra from biofilmed and cleaned samples to evaluate spectral shape variability within (intra-) and between (inter-) groups. The average intra-group spectral angle was less than the average inter-group spectral angle across the full spectrum (9.76°, 9.85° < 11.04°) (Table 1). This was also the case when comparing spectral shape for different parts of the spectrum, with the VIS (4.98°, 4.73° < 5.98°), NIR (4.47°, 4.32° < 4.49°), and SWIR (9.99°, 8.53° < 10.11°) all exhibiting lower average intra-group spectral angles than inter-group (Table 1). The difference in spectral angle was the lowest in the NIR region, with average intra-group biofilmed and intra-group cleaned spectral angle values differing by only 0.02° and 0.17° respectively from the inter-group spectral angle.

	Intra-group SA, damp biofilmed plastic (°)	Intra-group SA, damp cleaned plastic (°)	Inter-group SA, biofilmed vs cleaned (°)
Full Spectrum	9.76	9.85	11.04
VIS (400-700 nm)	4.98	4.73	5.98
NIR (700-1350 nm)	4.47	4.32	4.49
SWIR(1410-2350 nm)	9.99	8.53	10.11

Table 1: Average spectral angle of each unique pairwise combination of individual plastic reflectance measurements within (e.g. biofilmed vs biofilmed) and between (eg biofilmed + cleaned) measurement groups. A lower spectral angle indicates a greater degree of spectral shape similarity.

An average biofilm absorptance spectra, representing the fraction of light not reflected by biofilm, was estimated from reflectance measurements (Fig. 6B). Microplastic associated biofilms were found to absorb the most in the VIS with a narrow peak at 673 nm, followed by very low absorption in the NIR, and moderate absorption in the SWIR. Normalized biofilm absorptance at visible wavelengths shows broad absorption at blue wavelengths, a narrow absorption feature in the red at 673 nm, and lower absorptance in the green (Fig. 7A). These trends agree with normalized absorptance spectra of red and green snow algae from (Fig. 7B) calculated similarly (Khan et al., 2021).

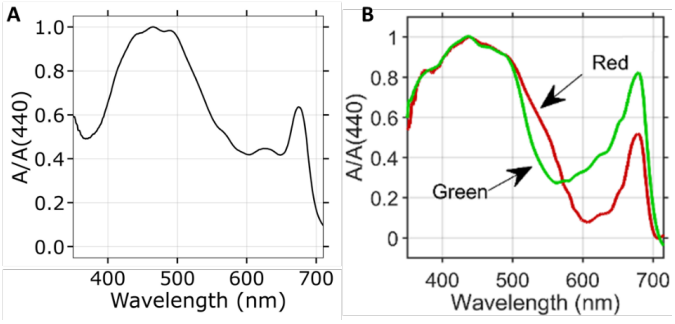

Figure 7: Normalized absorptance by microplastic biofilms from this study (A) vs normalized absorptance by red and green algae from Khan et al. 2021 (B) across the visible range.

The dry microplastic reflectance endmember determined in this study increases through the VIS and NIR to a maximum at 880 nm, and decreases into the SWIR, with a higher overall magnitude than the damp plastic spectra (Fig. 8). This new dry microplastic endmember is similar in spectral shape (θ=2.7) and magnitude to the previously reported endmember in (Garaba and Dierssen, 2018) collected from the North Atlantic.

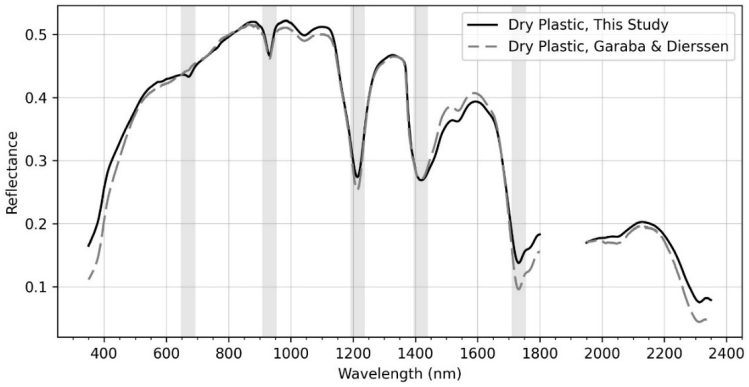

Figure 8: Average dry microplastic spectra from this study and from Garaba and Dierssen (2017). Grey bands indicate 673 nm chlorophyll-a absorption and the four characteristic plastic absorption features in the NIR/SWIR.

3.3 Remote Sensing Algorithms

Using the average biofilmed spectra from Fig. 6A, we conducted a sensitivity analysis to determine whether the presence of pigmented biofilms could influence the retrieval of chlorophyll-a from satellites. Linear mixing simulations of microplastic and water reflectance endmembers show increasing chlorophyll-a concentration values retrieved by the Color Index algorithm as the subpixel fractional coverage by plastic increases (Fig. 9). This is the case for simulations using both the biofilmed and cleaned microplastic reflectance endmembers. The

retrieved chlorophyll-a concentration deviates from the background value sooner when simulating with the biofilmed microplastic endmember than the cleaned microplastic endmember, surpassing the threshold of a 5% difference at a plastic concentration of 2.88×10^8 pieces/km^2 as opposed to 3.8×10^8 pieces/km^2.

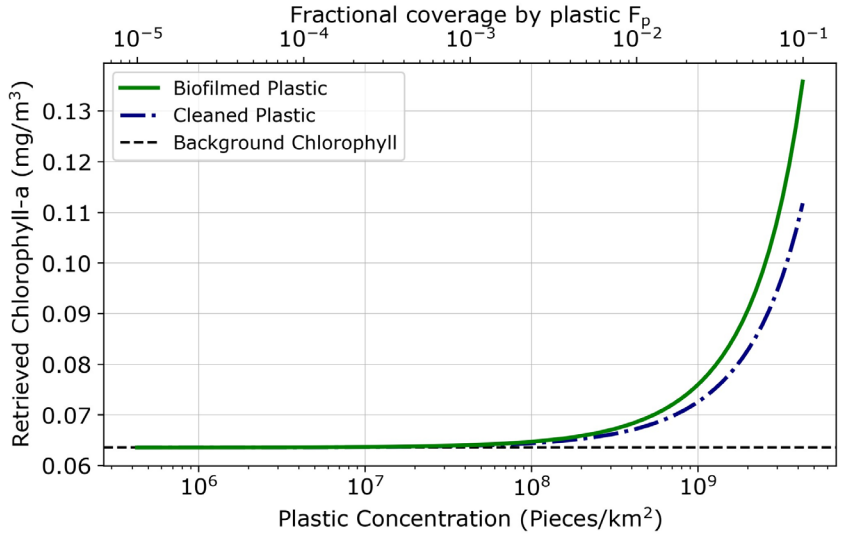

Figure 9: Retrieved chlorophyll-a concentration from simulated mixed-pixel spectra of varied plastic coverage conditions using the standard Color Index (CI) algorithm. The black line represents the chlorophyll-a concentration retrieved with no microplastic coverage (f_p=0), and the green and blue lines represent the retrieved chlorophyll-a concentration with variable surface microplastic concentrations, simulated using the biofilmed and cleaned microplastic endmembers respectively. At present, the greatest microplastic concentration observed in the GPGP is 1.2×10^7 pieces/km^2 from (Law et al. 2014).

4. Discussion

Relatively few studies have examined the topics of marine biofilm optical properties and marine biofilm community composition on their own, and to our knowledge, no prior study has examined the two concurrently. This is one of the first studies to quantify how natural biofilms from the oligotrophic ocean gyres impact the reflectance of floating marine microplastics and how this can impact remote sensing algorithms.

Biofilm abundance and community composition across the Ocean Gyre

Even with the small sample size, the genomic data indicates that biofilm is quite consistent across the convergence zone of the North Pacific gyre. The most abundant taxa in the microbiome analyses were the prokaryotic genus *Pseudoalteromonas*, and the eukaryotic genus *Tsunamia*, which made up 37.4% of the total prokaryotic microbiome and 52.9% of the total eukaryotic microbiome, respectively. The only photosynthetic prokayrotic organisms we observed occurred in low abundance, making up a combined 1.1 % of the prokaryotic microbiome. However, the majority of eukaryotic organisms were photosynthetic, including the abundant red algae *Tsunamia,* the photosynthetic stramenopile *Pinguiochrysis*, and the haptophyte *Exanthemachrysis.* The influence of these pigmented taxa is evident in both the reflectance and absorptance spectra. Due to broad absorption in the blue and a narrow absorption peak in the red, the reflectance is significantly lower in these portions of the visible spectrum for biofilmed microplastics compared to clean microplastics.

In addition to the regularity of biofilm community composition and spectral properties, biofilm mass abundance and beta-diversity analyses suggest that biofilms are rather uniform

within our study region. Principle coordinate analyses of Bray-Curtis dissimilarities did not reveal geographic trends in prokaryotic or eukaryotic biofilm beta-diversity (see Appendix 5), and biofilm mass abundance measurements were stable across the gyre. Thus, the biofilm properties we observed and their impact on floating microplastic pieces within the GPGP are relatively consistent, and can be used to better understand these pieces and their interactions with the marine environment.

Photosynthesis of Biofilm

Different photosynthetic organisms have been found to absorb light at slightly different wavelengths. In a recent paper, Summers et al. 2023 analyzed three species of snow algae: The green algae *Ulva sp.*, brown algae *S. Latissima,* and the red algae *P. palmata*. This study determined different absorption band centers in the red for each species, with the green, brown, and red algae absorption features being centered at 651, 664, and 672 nm, respectively (Summers et al., 2023). In our study, the red absorption feature of biofilms was centered at 673 nm and matches the characterization of red algae by Summers et al. 2023. This aligns with the observed abundance of the red algae *Tsunamia* as the dominate photosynthetic organism on these microplastics.

Plastic pieces in other regions, such as different subtropical gyres or in coastal or inland systems, will likely have biofilms dominated by other photosynthetic taxa. In these cases, hyperspectral remote sensing data may allow for the position of the absorption band center to be accurately determined, which can inform on the species constituting these biofilms. With hyperspectral ocean color missions such as Plankton, Aerosol, Cloud, ocean Ecosystem (PACE), Geostationary Littoral Imaging Radiometer (GLIMR), and Surface Biology and Geology (SBG)

launching in the next 5 years, future plastic remote sensing projects will be able to leverage unprecedented spectral resolution in the VIS/NIR to pinpoint the position of absorption features and gain additional insight into the photosynthetic systems on plastic pieces.

Impact on Algorithms to Detect Microplastics

In their 2018 study, Garaba and Dierssen noted of their dry microplastic pieces that they "were remarkably consistent in spectral properties with a general white appearance, similar magnitude and spectral shape across all size classes". Building on this, our study shows how consistent the floating microplastic properties are across the global ocean. Plastic samples used in our study were obtained at sea in the North Pacific gyre, while the pieces used in Garaba and Dierssen, 2018 originated from the western North Atlantic. Despite this, the dry microplastic endmember retrieved here aligns well with the average spectral reflectance reported in that study. Spectra obtained from the N. Pacific and N. Atlantic had very strong degree of spectral shape similarity (θ=2.7) and consistent spectral shape and magnitude (see Fig. 8). Analyses from the same study determined that different microplastic polymer compositions exhibited distinct reflectance properties, with the bulk dry microplastic signal most resembling polypropylene (PP), polyethylene terephthalate (PET), and low-density polyethylene (LDPE) (Garaba et al., 2018). The prominence of these three polymer types in marine microplastic samples has been independently observed in studies using FT-IR and Raman spectroscopy (Kanhai et al., 2017; Lenz et al., 2015). Hence, the high degree of similarity between the bulk, dry microplastic endmember of our study and that in (Garaba and Dierssen, 2018) suggests that the individual particles in both studies consist of the same types of polymers (LDPE, PET, and PP) in roughly the same proportions. With the context of where these particles were collected, it seems that the

same few plastic polymers make up a majority of plastic particles in both the north Pacific and north Atlantic subtropical gyres. This may be a result of polymer characteristics such as buoyancy and durability, physical transport mechanisms of plastics into these gyres, a manufacturing preference towards the production of these polymers, or a combination of the three.

Algorithms have been developed for the remote sensing of marine plastics that use line height indexes and ratio indexes to target hydrocarbons in remote sensing imagery. In a recent paper, Castagna et al. (2023) analyzed seven different algorithms to identify plastics on land and floating on aquatic ecosystems. Notably, five of the seven algorithms rely on reflectance values at or near the 1215 or 1732 nm wavelengths associated with plastic absorption (Castagna et al., 2023). These wavelengths are desirable for plastic remote sensing not only because of the presence of plastic absorption features but also because of their presence within atmospheric windows. Near these wavelengths the atmosphere does not absorb strongly, which enables high signal-to-noise ratio measurements to be made by remote sensing systems (Garaba and Dierssen, 2018). The 1215 and 1732 nm absorption features are also interesting based on our analyses because the band depth at these wavelengths was not influenced by whether the microplastic pieces are biofilmed or not. Going forward, we expect that algorithms using these wavelengths will not be sensitive to the degree of biofilming on target plastic pieces. This may permit consistency in algorithm retrievals across different ecosystems where plastics may be subject to different amounts and types of biofilm.

Microplastics and biofilm impact on ocean color remote sensing

Currently, ocean color near-surface chlorophyll-a concentration products have a variety of applications, including the study of basin-scale primary productivity, algorithm tuning, and global ocean modelling (Campbell et al., 2002; Gregg, 2008; Xing and Boss, 2021). Within these contexts, near-surface chlorophyll-a products characterize the pigments associated with free-floating phytoplankton, but are not designed to inform on substrate bound, pigmented systems such as microplastic biofilms (Marañón, 2009; O'Reilly et al., 1998). With the prolonged mission cycle of MODIS-Aqua, over 20 years of consistent ocean color and chlorophyll-a measurements are available; data which has become a promising target for studying climate change impacts. Recent work has identified that in much of the global tropics and subtropics, low interannual variability in ocean color and chlorophyll-a retrievals permit a high enough SNR for the identification of climate change driven trends (Cael et al., 2022). However, these oligotrophic regions are the same regions that have convergence zones with high plastic concentrations. Hu et al. mentioned how plastics are "white" bits of sea surface, but the spectra show that they absorb blue light and reflect in such a manner that they could also impact the chlorophyll retrievals at high concentrations (Hu et al., 2019). This is observation led us to conduct mixed-pixel simulations to determine at what concentration biofilmed marine microplastics may influence ocean color chlorophyll-a retrievals, with the goal of confirming that trends in these regions are not influenced by surface microplastics. In these simulations, a surface plastic concentration of 2.88×10^8 pieces/km^2 was required to obtain a 5% error in chlorophyll-a retrieval (See Fig. 9). Field studies between 2001 and 2012 observed typical surface plastic concentrations between 10^4 and 10^6 within the Great Pacific Garbage Patch, so it is unlikely that the presence of surface microplastics in the environment are routinely impacting

chlorophyll-a retrievals at present (Law et al., 2014). However, environmental plastic concentrations as high as $1.2x10^7$ pieces/km^2 have been observed along "parallel 'rivers' of highly visible debris that were meters in width and extended to the horizon" within the GPGP (Law et al., 2014). This small-scale feature of plastic concentration is thought to be associated with high-frequency internal waves, and other features, such as Langmuir circulation and submesoscale fronts have also been proposed as drivers of extremely high plastic concentration along meter-scale features (Sebille et al., 2020). Very high spatial resolution data such as that from drones or airborne platforms may observe sufficiently high plastic concentrations along these small spatial scale features to noticeably impact chlorophyll-a measurements.

Future Outlook

Surface plastic concentrations are highly variable across ocean gyres, and individual in-situ observations are determined by a complex combination of large and small scale physical oceanographic processes along with contributions by discrete litter events. Because of this complexity, there is a need to develop more monitoring techniques to better understand the spatial and temporal variability of floating microplastics. This study suggests that plastics are not yet concentrated enough for satellite-based detection, but we do observe distinct optical properties that may have applications to other remote sensing platforms. Future remote sensing implementations for microplastic studies focusing on visible wavelengths will need to better constrain the optical properties of biofilms on plastics. Understanding the biofilm communities in other convergence zones, such as in the Southern hemisphere, for example, could be an important next step. Plastics in the environment have their reflectance modified by these natural biofilms, so cleaned and/or virgin microplastic endmembers will not sufficiently characterize

practical microplastic reflectance for some applications. However, approaches in the NIR/SWIR will be more robust to biofilm based on the consistency of absorption band depth. Going forward these spectral measurements of biofilmed microplastic reflectance are applicable to radiative transfer simulations, and may ultimately inform on thresholds for the direct detection of microplastics.

Appendices

Appendix 1: Example of aggregated biofilmed microplastic pieces collected during this study.

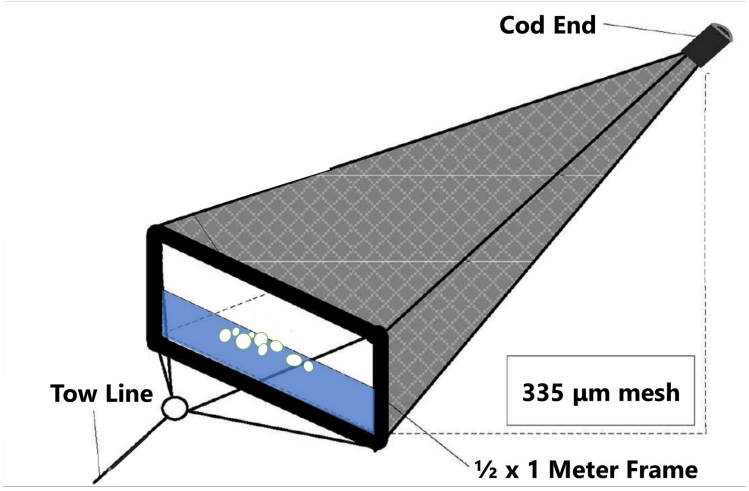

Appendix 2: Diagram of neuston net tow deployment.

Appendix 3: Photograph of the reflectance measurement procedure.

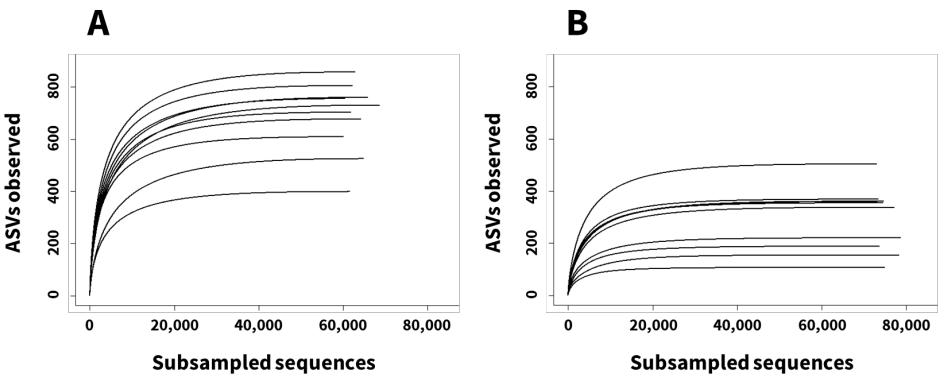

Appendix 4: Rarefaction curves for the prokaryotic analysis (A) and eukaryotic analysis (B). Curves were produced by the rarecurve command in phyloseq, with a step size of 25. Note that each curve saturates prior to termination.

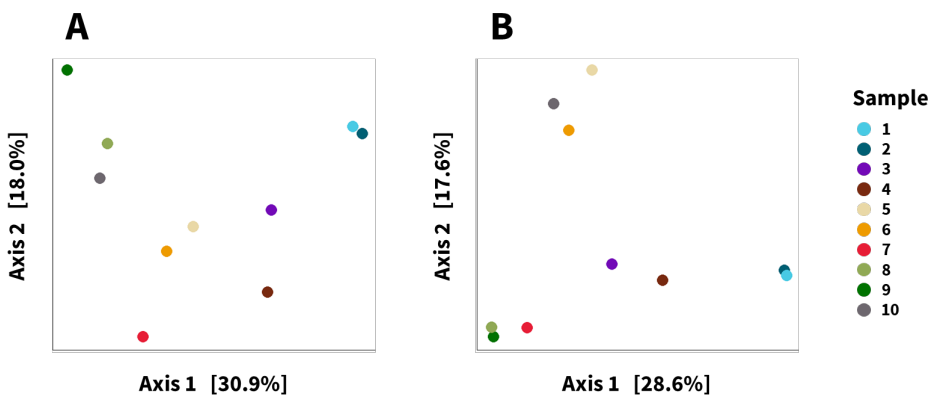

Appendix 5: Ordinations displaying principal coordinates analysis on Bray-Curtis dissimilarities from the prokaryotic community compositions (A) and eukaryotic compositions (B). Microbial communities are colored according to sample identity.

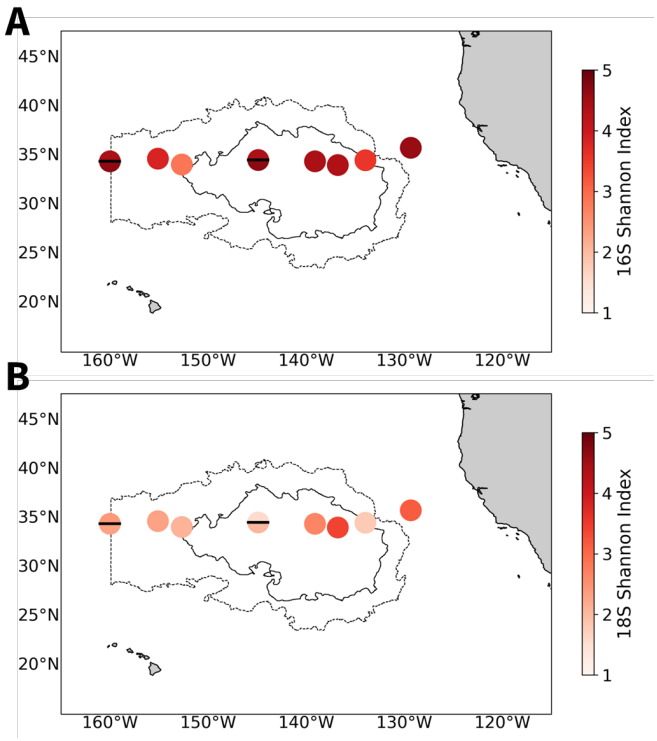

Appendix 6: Sample alpha diversity using the Shannon Diversity Index for the prokaryotic (A) and eukaryotic (B) analysis. Co-located samples are represented with half-circles.

Plastic Batch	Latitude	Longitude	mg biofilm/g microplastic
7_1	29.01578333	-159.2098	0.205
7_3	32.65918333	-159.820433	2.078
7_7_B2	34.12206667	-152.681483	7.827
7_7_B3	34.12206667	-152.681483	8.619
7_8_B1	34.73708333	-150.482483	1.863
7_8_B2	34.73708333	-150.482483	6.570
7_9	34.12343333	-147.5362	6.142
7_13	34.07301667	-136.767467	13.798
7_12	34.43418333	-139.0954	21.174
7_14_B1	34.55565	-133.973617	10.258
7_10_B2	34.57161667	-144.900917	7.347
7_10_B2	34.57161667	-144.900917	14.436
7_11	34.59306667	-142.150117	22.065
7_15	35.50921667	-131.175333	15.447
7_15	35.50921667	-131.175333	6.532
7_16	35.82983333	-129.328933	4.259
7_17	35.62028333	-131.099767	5.118

Appendix 7: Dry mass of biofilm per dry mass of microplastic (mg/g) recorded for samples in this study.

References

Cael, B.B., Bisson, K., Boss, E., Dutkiewicz, S., Henson, S., 2022. Global climate change trends detected in indicators of ocean ecology.

Callahan, B.J., McMurdie, P.J., Rosen, M.J., Han, A.W., Johnson, A.J.A., Holmes, S.P., 2016. DADA2: High-resolution sample inference from Illumina amplicon data. Nat Methods 13, 581–583. https://doi.org/10.1038/nmeth.3869

Campbell, J., Antoine, D., Armstrong, R., Arrigo, K., Balch, W., Barber, R., Behrenfeld, M., Bidigare, R., Bishop, J., Carr, M.-E., Esaias, W., Falkowski, P., Hoepffner, N., Iverson, R., Kiefer, D., Lohrenz, S., Marra, J., Morel, A., Ryan, J., Vedernikov, V., Waters, K., Yentsch, C., Yoder, J., 2002. Comparison of algorithms for estimating ocean primary production from surface chlorophyll, temperature, and irradiance. Global Biogeochemical Cycles 16, 9-1-9–15. https://doi.org/10.1029/2001GB001444

Carpenter, E.J., Smith Jr, K., 1972. Plastics on the Sargasso Sea surface. Science 175, 1240–1241.

Castagna, A., Dierssen, H.M., Devriese, L.I., Everaert, G., Knaeps, E., Sterckx, S., 2023. Evaluation of historic and new detection algorithms for different types of plastics over land and water from hyperspectral data and imagery. Remote Sensing of Environment 298, 113834. https://doi.org/10.1016/j.rse.2023.113834

Castagna, A., Johnson, B.C., Voss, K., Dierssen, H.M., Patrick, H., Germer, T.A., Sabbe, K., Vyverman, W., 2019. Uncertainty in global downwelling plane irradiance estimates from sintered polytetrafluoroethylene plaque radiance measurements. Appl. Opt., AO 58, 4497–4511. https://doi.org/10.1364/AO.58.004497

Clark, R.N., Roush, T.L., 1984. Reflectance spectroscopy: Quantitative analysis techniques for remote sensing applications. Journal of Geophysical Research: Solid Earth 89, 6329–6340.

Colton, J.B., Burns, B.R., Knapp, F.D., 1974. Plastic Particles in Surface Waters of the Northwestern Atlantic. Science 185, 491–497. https://doi.org/10.1126/science.185.4150.491

Cózar, A., Aliani, S., Basurko, O.C., Arias, M., Isobe, A., Topouzelis, K., Rubio, A., Morales-Caselles, C., 2021. Marine Litter Windrows: A Strategic Target to Understand and Manage the Ocean Plastic Pollution. Frontiers in Marine Science 8.

Debeljak, P., Pinto, M., Proietti, M., Reisser, J., F. Ferrari, F., Abbas, B., Loosdrecht, M.C.M. van, Slat, B., J. Herndl, G., 2017. Extracting DNA from ocean microplastics: a method comparison study. Analytical Methods 9, 1521–1526. https://doi.org/10.1039/C6AY03119F

Dierssen, H.M., 2019. Hyperspectral Measurements, Parameterizations, and Atmospheric Correction of Whitecaps and Foam From Visible to Shortwave Infrared for Ocean Color Remote Sensing. Frontiers in Earth Science 7.

Frye, H. 2023. Novel Hyperspectral Approaches to Quantifying Taxonomic and Functional Diversity in Terrestrial Ecosystems. University of Connecticut Doctoral Dissertations.

Garaba, S., Dierssen, H., 2017. Spectral reference library of 11 types of virgin plastic pellets common in marine plastic debris. Data Set.

Garaba, S.P., Aitken, J., Slat, B., Dierssen, H.M., Lebreton, L., Zielinski, O., Reisser, J., 2018. Sensing Ocean Plastics with an Airborne Hyperspectral Shortwave Infrared Imager. Environ. Sci. Technol. 52, 11699–11707. https://doi.org/10.1021/acs.est.8b02855

Garaba, S.P., Dierssen, H.M., 2020. Hyperspectral ultraviolet to shortwave infrared characteristics of marine-harvested, washed-ashore and virgin plastics. Earth System Science Data 12, 77–86. https://doi.org/10.5194/essd-12-77-2020

Garaba, S.P., Dierssen, H.M., 2018. An airborne remote sensing case study of synthetic hydrocarbon detection using short wave infrared absorption features identified from marine-harvested macro- and microplastics. Remote Sensing of Environment 205, 224–235. https://doi.org/10.1016/j.rse.2017.11.023

Gregg, W.W., 2008. Assimilation of SeaWiFS ocean chlorophyll data into a three-dimensional global ocean model. Journal of Marine Systems, Physical-Biological Interactions in the Upper Ocean 69, 205–225. https://doi.org/10.1016/j.jmarsys.2006.02.015

Hu, C., 2021. Remote detection of marine debris using satellite observations in the visible and near infrared spectral range: Challenges and potentials. Remote Sensing of Environment 259, 112414. https://doi.org/10.1016/j.rse.2021.112414

Hu, C., Feng, L., Lee, Z., Franz, B.A., Bailey, S.W., Werdell, P.J., Proctor, C.W., 2019. Improving Satellite Global Chlorophyll a Data Products Through Algorithm Refinement and Data Recovery. Journal of Geophysical Research: Oceans 124, 1524–1543. https://doi.org/10.1029/2019JC014941

Hueni, A., Bialek, A., 2017. Cause, Effect, and Correction of Field Spectroradiometer Interchannel Radiometric Steps. IEEE Journal of Selected Topics in Applied Earth Observations and Remote Sensing 10, 1542–1551. https://doi.org/10.1109/JSTARS.2016.2625043

Jambeck, J.R., Geyer, R., Wilcox, C., Siegler, T.R., Perryman, M., Andrady, A., Narayan, R., Law, K.L., 2015. Plastic waste inputs from land into the ocean. Science 347, 768–771. https://doi.org/10.1126/science.1260352

Kazemipour, F., Méléder, V., Launeau, P., 2011. Optical properties of microphytobenthic biofilms (MPBOM): Biomass retrieval implication. Journal of Quantitative Spectroscopy and Radiative Transfer 112, 131–142.

Khan, A.L., Dierssen, H.M., Scambos, T.A., Höfer, J., Cordero, R.R., 2021. Spectral characterization, radiative forcing and pigment content of coastal Antarctic snow algae: approaches to spectrally discriminate red and green communities and their impact on snowmelt. The Cryosphere 15, 133–148.

Kirk, J.T.O., 1994. Light and Photosynthesis in Aquatic Ecosystems. Cambridge University Press.

Kruse, F.A., Lefkoff, A., Boardman, J., Heidebrecht, K., Shapiro, A., Barloon, P., Goetz, A., 1993. The spectral image processing system (SIPS)—interactive visualization and analysis of imaging spectrometer data. Remote sensing of environment 44, 145–163.

Langstroth, Lovell, Langstroth, Libby, 2000. A Living Bay: The Underwater World of Monterey Bay. University of California Press.

Latva, M., Zadjelovic, V., Wright, R., 2021. Current Research on Microbe-Plastic Interactions in the Marine Environment. https://doi.org/10.20944/preprints202107.0273.v1

Law, K.L., 2017. Plastics in the Marine Environment. Annual Review of Marine Science 9, 205–229. https://doi.org/10.1146/annurev-marine-010816-060409

Law, K.L., Morét-Ferguson, S., Maximenko, N.A., Proskurowski, G., Peacock, E.E., Hafner, J., Reddy, C.M., 2010. Plastic Accumulation in the North Atlantic Subtropical Gyre. Science 329, 1185–1188. https://doi.org/10.1126/science.1192321

Law, K.L., Morét-Ferguson, S.E., Goodwin, D.S., Zettler, E.R., DeForce, E., Kukulka, T., Proskurowski, G., 2014. Distribution of surface plastic debris in the eastern Pacific Ocean from an 11-year data set. Environmental science & technology 48, 4732–4738.

Lebreton, L., Slat, B., Ferrari, F., Sainte-Rose, B., Aitken, J., Marthouse, R., Hajbane, S., Cunsolo, S., Schwarz, A., Levivier, A., Noble, K., Debeljak, P., Maral, H., Schoeneich-Argent, R., Brambini, R., Reisser, J., 2018. Evidence that the Great Pacific Garbage Patch is rapidly accumulating plastic. Scientific Reports 8, 4666. https://doi.org/10.1038/s41598-018-22939-w

Love, M.I., Huber, W., Anders, S., 2014. Moderated estimation of fold change and dispersion for RNA-seq data with DESeq2. Genome Biology 15, 550. https://doi.org/10.1186/s13059-014-0550-8

Magoč, T., Salzberg, S.L., 2011. FLASH: fast length adjustment of short reads to improve genome assemblies. Bioinformatics 27, 2957–2963. https://doi.org/10.1093/bioinformatics/btr507

Marañón, E., 2009. Phytoplankton Size Structure, in: Steele, J.H. (Ed.), Encyclopedia of Ocean Sciences (Second Edition). Academic Press, Oxford, pp. 445–452. https://doi.org/10.1016/B978-012374473-9.00661-5

Marrs, S.J., Head, R.M., Cowling, M.J., Hodgkiess, T., Davenport, J., 1999. Spectrophotometric Evaluation of Micro-algal Fouling on Marine Optical Windows. Estuarine, Coastal and Shelf Science 48, 137–141. https://doi.org/10.1006/ecss.1998.0407

Maximenko, N., Corradi, P., Law, K.L., Van Sebille, E., Garaba, S.P., Lampitt, R.S., Galgani, F., Martinez-Vicente, V., Goddijn-Murphy, L., Veiga, J.M., 2019. Toward the integrated marine debris observing system. Frontiers in marine science 6, 447.

McMurdie, P.J., Holmes, S., 2014. Waste Not, Want Not: Why Rarefying Microbiome Data Is Inadmissible. PLOS Computational Biology 10, e1003531. https://doi.org/10.1371/journal.pcbi.1003531

McMurdie, P.J., Holmes, S., 2013. phyloseq: An R Package for Reproducible Interactive Analysis and Graphics of Microbiome Census Data. PLOS ONE 8, e61217. https://doi.org/10.1371/journal.pone.0061217

Mobley, C.D., 1999. Estimation of the remote-sensing reflectance from above-surface measurements. Appl. Opt., AO 38, 7442–7455. https://doi.org/10.1364/AO.38.007442

NASA Ocean Biology Processing Group, 2023. Spectral Characterization Data by Sensor. Retrieved from https://oceancolor.gsfc.nasa.gov/resources/docs/rsr_tables/

O'Reilly, J.E., Maritorena, S., Mitchell, B.G., Siegel, D.A., Carder, K.L., Garver, S.A., Kahru, M., McClain, C., 1998. Ocean color chlorophyll algorithms for SeaWiFS. Journal of Geophysical Research: Oceans 103, 24937–24953. https://doi.org/10.1029/98JC02160

O'Reilly, J.E., Werdell, P.J., 2019. Chlorophyll algorithms for ocean color sensors - OC4, OC5 & OC6. Remote Sensing of Environment 229, 32–47. https://doi.org/10.1016/j.rse.2019.04.021

Pertea, G. 2018. gpertea/fqtrim: fqtrim release v0.9.7. doi:10.5281/zenodo.1185412.

Pinto, M., Langer, T.M., Hüffer, T., Hofmann, T., Herndl, G.J., 2019. The composition of bacterial communities associated with plastic biofilms differs between different polymers and stages of biofilm succession. PLOS ONE 14, e0217165. https://doi.org/10.1371/journal.pone.0217165

Quast, C., Pruesse, E., Yilmaz, P., Gerken, J., Schweer, T., Yarza, P., Peplies, J., Glöckner, F.O., 2013. The SILVA ribosomal RNA gene database project: improved data processing and web-based tools. Nucleic Acids Research 41, D590–D596. https://doi.org/10.1093/nar/gks1219

Rognes, T., Flouri, T., Nichols, B., Quince, C., Mahé, F., 2016. VSEARCH: a versatile open source tool for metagenomics. PeerJ 4, e2584. https://doi.org/10.7717/peerj.2584

Scafutto, R.D.P.M., Van Der Werff, H., Bakker, W.H., Van Der Meer, F., Roberto De Souza Filho, C., 2021. Assessing Scientific and Industry Grade SWIR Airborne Imaging Spectrometers for CH_4 Mapping, in: 2021 IEEE International Geoscience and Remote Sensing Symposium IGARSS. Presented at the IGARSS 2021 - 2021 IEEE International Geoscience and Remote Sensing Symposium, IEEE, Brussels, Belgium, pp. 1871–1874. https://doi.org/10.1109/IGARSS47720.2021.9554544

Sebille, E. van, Aliani, S., Law, K.L., Maximenko, N., Alsina, J.M., Bagaev, A., Bergmann, M., Chapron, B., Chubarenko, I., Cózar, A., Delandmeter, P., Egger, M., Fox-Kemper, B., Garaba, S.P., Goddijn-Murphy, L., Hardesty, B.D., Hoffman, M.J., Isobe, A., Jongedijk, C.E., Kaandorp, M.L.A., Khatmullina, L., Koelmans, A.A., Kukulka, T., Laufkötter, C., Lebreton, L., Lobelle, D., Maes, C., Martinez-Vicente, V., Maqueda, M.A.M., Poulain-Zarcos, M., Rodríguez, E., Ryan, P.G., Shanks, A.L., Shim, W.J., Suaria, G., Thiel, M., Bremer, T.S. van den, Wichmann, D., 2020. The physical oceanography of the transport of floating marine debris. Environ. Res. Lett. 15, 023003. https://doi.org/10.1088/1748-9326/ab6d7d

Somers, B., Asner, G.P., Tits, L., Coppin, P., 2011. Endmember variability in Spectral Mixture Analysis: A review. Remote Sensing of Environment 115, 1603–1616. https://doi.org/10.1016/j.rse.2011.03.003

Summers, N., Fragoso, G.M., Johnsen, G., 2023. Photophysiologically active green, red, and brown macroalgae living in the Arctic Polar Night. Sci Rep 13, 17971. https://doi.org/10.1038/s41598-023-44026-5

Thevenon, F., Carroll, C., Sousa, J. (Eds.), 2015. Plastic debris in the ocean: the characterization of marine plastics and their environmental impacts, situation analysis report. International Union for Conservation of Nature. https://doi.org/10.2305/IUCN.CH.2014.03.en

Topouzelis, K., Papakonstantinou, A., Garaba, S.P., 2019. Detection of floating plastics from satellite and unmanned aerial systems (Plastic Litter Project 2018). International Journal of Applied Earth Observation and Geoinformation 79, 175–183.

Van Sebille, E., Wilcox, C., Lebreton, L., Maximenko, N., Hardesty, B.D., Van Franeker, J.A., Eriksen, M., Siegel, D., Galgani, F., Law, K.L., 2015. A global inventory of small floating plastic debris. Environmental Research Letters 10, 124006.

West, J.A., Hansen, G.I., Hanyuda, T., Zuccarello, G.C., West, J.A., Hansen, G.I., Hanyuda, T., Zuccarello, G.C., 2016. Flora of drift plastics: a new red algal genus, <italic>Tsunamia transpacifica</italic> (Stylonematophyceae) from Japanese tsunami debris in the northeast Pacific Ocean. Algae 31, 289–301. https://doi.org/10.4490/algae.2016.31.10.20

Wickham, Hadley., 2016. Ggplot2 : elegant graphics for data analysis /. Springer, New York :

Wright, R.J., Langille, M.G.I., Walker, T.R., 2021. Food or just a free ride? A meta-analysis reveals the global diversity of the Plastisphere. ISME J 15, 789–806. https://doi.org/10.1038/s41396-020-00814-9

Xing, X., Boss, E., 2021. Chlorophyll-Based Model to Estimate Underwater Photosynthetically Available Radiation for Modeling, In-Situ, and Remote-Sensing Applications. Geophysical Research Letters 48, e2020GL092189. https://doi.org/10.1029/2020GL092189

Zettler, E.R., Mincer, T.J., Amaral-Zettler, L.A., 2013. Life in the “Plastisphere”: Microbial Communities on Plastic Marine Debris. Environ. Sci. Technol. 47, 7137–7146. https://doi.org/10.1021/es401288x